ANALYSIS OF RADIAL RADIOGRAPHY FOR THE LINER STABILITY SERIES AT PEGASUS: PGII-59, PGII-62, AND PGII-63

Dane V. Morgan, David Platts, Jack S. Shlachter,
Donald L. Martinez, and Bernard Carpenter
Los Alamos National Laboratory, Los Alamos, NM 87545

Abstract

Recently, three liner stability experiments were performed at the Pegasus II pulsed power facility to determine the asymmetric variations in the material density of a cylindrical liner during an electro-magnetically driven implosion. The initial campaign consisted of three experiments, designated LS-1, LS-2, and LS-3. LS-1 and LS-2 were driven with a peak current of approximately 4.2 MA, whereas the peak current for LS-3 was approximately 6.4 MA. All three liners initially were 0.4 mm wall aluminum cylinders with a mean radius of 2.38 cm and a height of 2.0 cm. The inner surface of each liner was coated with a thin (18-23 μm) layer of gold to aid in the determination of the position of the inner surface of the liner. Radial radiography was used to characterize the z-dependent and θ-dependent instabilities that were observed as the liner contracted.

Introduction

Liner instabilities are a major issue for developing pulsed power to drive cylindrically symmetric implosions. We have therefore undertaken a campaign of liner stability experiments to quantitatively determine the non-uniformities and deviations from cylindrical symmetry of aluminum liners as they implode. In this paper, we estimate the material density variations with time, and show how the z-dependent low density regions (or bubbles) affect the inside surface of the liner. We will also characterize the distribution of spatial wavelengths of the θ-dependent wrinkling or "crenelation" that grows on the inside surface of the imploding liner.

Dynamic x-ray radiography is an excellent diagnostic for observing the density variations of an imploding liner. The x-rays provide an inherent advantage over optical imaging systems, which are only capable of observing the outside surface of the liner, and these optical images may be obscured at late time by the formation of a plasma arc. X-ray imaging is especially useful because material densities can be determined quantitatively by measuring the x-ray transmission through the liner. The x-ray transmission is given as

$$\frac{I}{I_0} = \prod_{i=1}^{N} \left\{ \exp - \left[\left(\frac{\mu}{\rho} \right)_i \rho_i x_i \right] \right\}, \qquad [1]$$

where μ/ρ is the mass attenuation coefficient, ρ is the density, and x is the path length through material i, for a given x-ray energy $h\nu$. For these experiments, N=2, because two different materials were used: gold and aluminum. The mass attenuation coefficient is strongly dependent on both the atomic number and the x-ray energy[1], and therefore an accurate estimate of the x-ray spectrum is necessary for a valid analysis of the x-ray images. Because the x-ray

0-7803-4214-3/97/$10.00 © 1997 IEEE

Report Documentation Page

Form Approved
OMB No. 0704-0188

1. REPORT DATE	2. REPORT TYPE	3. DATES COVERED
JUN 1997	**N/A**	**-**

4. TITLE AND SUBTITLE
Analysis Of Radial Radiography For The Liner Stability Series At Pegasus: PGII-59, PGII-62, and PGII-63

5a. CONTRACT NUMBER
5b. GRANT NUMBER
5c. PROGRAM ELEMENT NUMBER

6. AUTHOR(S)

5d. PROJECT NUMBER
5e. TASK NUMBER
5f. WORK UNIT NUMBER

7. PERFORMING ORGANIZATION NAME(S) AND ADDRESS(ES)
Los Alamos National Laboratory, Los Alamos, NM 87545

8. PERFORMING ORGANIZATION REPORT NUMBER

9. SPONSORING/MONITORING AGENCY NAME(S) AND ADDRESS(ES)

10. SPONSOR/MONITOR'S ACRONYM(S)
11. SPONSOR/MONITOR'S REPORT NUMBER(S)

12. DISTRIBUTION/AVAILABILITY STATEMENT
Approved for public release, distribution unlimited

13. SUPPLEMENTARY NOTES
See also ADM002371. 2013 IEEE Pulsed Power Conference, Digest of Technical Papers 1976-2013, and Abstracts of the 2013 IEEE International Conference on Plasma Science. Held in San Francisco, CA on 16-21 June 2013. U.S. Government or Federal Purpose Rights License.

14. ABSTRACT
Recently, three liner stability experiments were performed at the Pegasus II pulsed power facility to determine the asymmetric variations in the material density of a cylindrical liner during an electro-magnetically driven implosion. The initial campaign consisted of three experiments, designated LS-1, N-2, and LS-3. LS- 1 and LS-2 were driven with a peak current of approximately 4.2 MA, whereas the peak current for LS-3 was approximately 6.4 MA. All three liners initially were 0.4 mm wall aluminum cylinders with a mean radius of 2.38 cm and a height of 2.0 cm. The inner surface of each liner was coated with a thin (18-23 ~m) layer of gold to aid in the determination of the position of the inner surface of the liner. Radial radiography was used to characterize the z-dependent and @dependent instabilities that were observed as the liner contracted.

15. SUBJECT TERMS

16. SECURITY CLASSIFICATION OF:			17. LIMITATION OF ABSTRACT	18. NUMBER OF PAGES	19a. NAME OF RESPONSIBLE PERSON
a. REPORT	b. ABSTRACT	c. THIS PAGE			
unclassified	**unclassified**	**unclassified**	**SAR**	**6**	

Standard Form 298 (Rev. 8-98)
Prescribed by ANSI Std Z39-18

sources used in these experiments emit a broad band of x-ray energies, Eq. [1] must be integrated over the entire x-ray spectrum.

If cylindrical symmetry is maintained during the liner implosion, ρ_i is a function of the distance from the center of the cylinder, r, and $\rho_i x_i$ from Eq. [1] is given as

$$\rho_i x_i = 2 \int_{r>L} \rho_i(r) \frac{rdr}{\sqrt{r^2 - L^2}}, \qquad [2]$$

for x-rays passing an offset distance L away from the axis of symmetry. The parameter L is proportional to the horizontal film coordinate. Model images can be generated from Eq. [1] and Eq. [2] if the blur effects are considered, and the non-linear conversion from x-ray intensity to film density is performed.

Characterization of the Radial Flash X-ray Radiographic System

For all three liner stability experiments, LS-1, LS-2, and LS-3, three flash x-ray units, radially oriented at 60° intervals, were utilized to generate images on film. These flash x-ray units have been described in detail by Platts *et al*[2]. The x-ray flash duration for each source was approximately 10 ns FWHM. Radiographic timing was established by planar vacuum photodiodes with plastic fluors located adjacent to each x-ray source. The images were observed on single-sided orthochromatic GWL film, which was located in contact with a Lanex Regular[3] x-ray-to-light intensifier screen, inside a light-tight film pack. The image magnification ranged between 1.21 and 1.26 for the three lines of sight. These dynamic radiographic images allowed us to observe the liner as it contracted, providing the principal diagnostic for these experiments.

A comprehensive analysis of the flash x-ray system must include estimates for the effective x-ray spectrum. The three "pulsed" x-ray sources emit tungsten line and Bremsstrahlung x-rays with a maximum endpoint energy of approximately 270 keV. Our x-ray spectral characterization of these x-ray systems also includes estimates for the x-ray absorption of the x-ray-to-light converter screen as a function of photon energy, the x-ray-to-light conversion efficiency, and the absorption of the film pack and film protective materials. The resulting "effective" x-ray spectrum is shown in Fig. 1. The effective spectrum has been calibrated with test radiographs of gold and aluminum step-wedges.

Another important issue for the characterization of our radiographic system is the line spread function (LSF), or "blur", which limits the resolution of the x-ray system at short spatial wavelengths. The LSF is described in the Fourier transform domain as the modulation transfer function (MTF). The most important factors causing the blur are the penumbra associated with the spot size of the x-ray source, and the diffusion of light from the fluorescent x-ray-to-light converter screen onto the film. Another important factor contributing to the blur is the generation of secondary x-ray radiation following K shell excitation of high-Z material in the fluorescent screen. A knife-edge experiment was performed to obtain the line spread function and the MTF for our x-ray systems. This method has been described by Watson *et al*[4]. The knife-edge data were differentiated to give an experimental LSF, and a least-squares fit of a Gaussian function to the experimental LSF was performed. The MTF for the experimental LSF and the Gaussian function are shown in Fig. 2. The LSF was then convolved with the x-ray

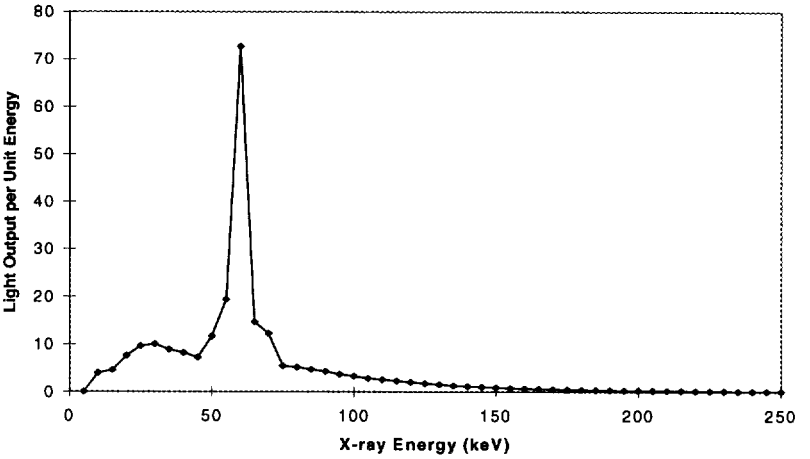

Fig. 1. *Effective X-ray Spectrum.*

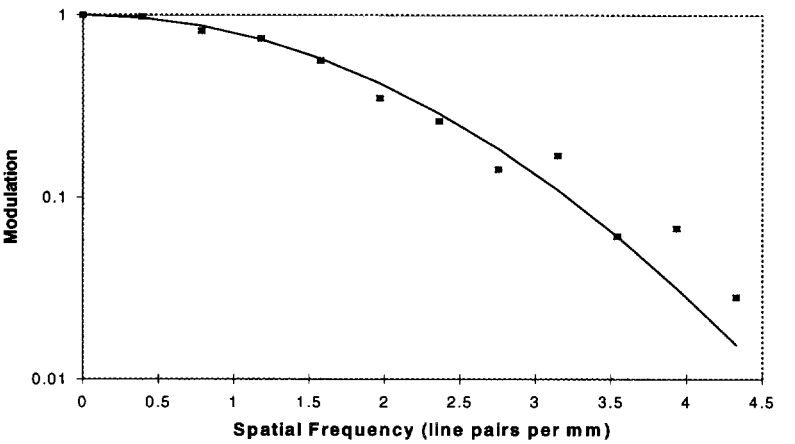

Fig. 2. *Modulation Transfer Function. The smooth line represents an FFT of a least-squares Gaussian fit to the Line Spread Function. The data points represent the experimental MTF.*

intensity distribution and converted to film density with the appropriate optical step-wedge sensitometry data to generate model radiographs.

Analysis of the θ-Dependent Instabilities

The θ-dependent instabilities were observed for all three experiments, LS-1, LS-2, and LS-3, generally for liner radial positions in the range $0.25R_o < r < 0.75R_o$. These instabilities were not observed at late times, where the liner radius became small ($r < 0.25R_o$), because the high density of materials caused the compressed liner to become opaque to our x-ray sources. θ-dependent instabilities were observed as vertically oriented streaks, or "crenelation", in the radiograph. Fig. 3 shows the second dynamic flash radiograph on LS-2, taken 13.7 μs after current start, which clearly shows the crenelation. For LS-1 and LS-2, the peak drive current was approximately 4.2 MA. In these two experiments, the magnitude of the crenelation increased with time as the liner contracted. These streaks appear strongest near the center of the radiograph and gradually diminish towards the liner edges because of the cylindrical geometry.

A line-out of the image in Fig. 3 is shown in Fig. 4, along with a model calculation. The experimental line-out shows magnitude of the variations associated with the crenelation. A discrete Fourier transform of the "crenelation" horizontal line-outs averaged over the entire length of the cylinder is compared with the MTF in Fig. 5. The FFT gives no indication of a characteristic wavelength associated with the θ-dependent instabilities, and therefore suggests that the irregularities are random in nature. A Monte-Carlo calculation shows that the gold inner layer is responsible for the crenelation because the amplitude of the oscillations can only be accounted for by random variations in the gold thickness.

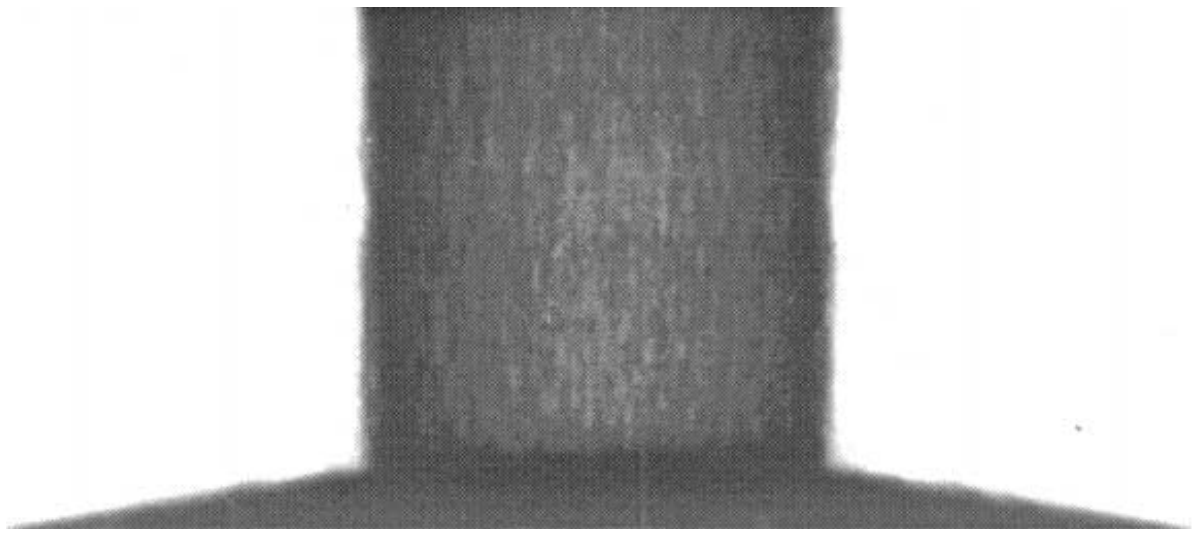

Fig. 3. *Flash radiograph of the LS-2 liner 13.7 μs after current start. The liner has contracted to approximately 31% of its initial radius. The vertically oriented streaks, or "crenelation", are clearly visible.*

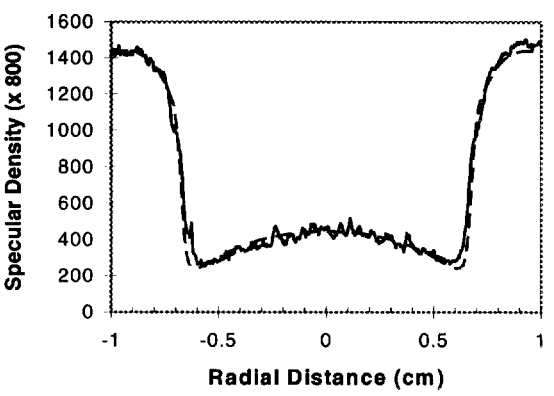

Fig. 4. *Horizontal Line-out of Fig. 3 at the midplane (solid line). Model calculation (dashed line).*

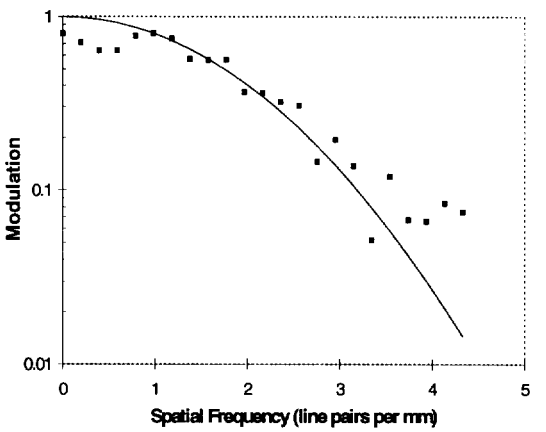

Fig. 5. *FFT of the crenelation (squares) compared with the system MTF (solid line).*

Analysis of z-Dependent Instabilities

At higher drive currents, z-dependent "bubbles" begin to form on the outside surface of the liner as it moves inward. LS-3 radiograph #2, shown in Fig. 6, was observed 8.5 μsec after current start, with a peak drive current of 6.4 MA. This radiograph shows the z-dependent instabilities typically observed in aluminum liners at high drive current. These onset of the formation of the bubbles appears to be associated with the melt of the aluminum on the outside surface of the liner. One purpose of these experiments was to determine the location of the inside of the liner surface as a function of z as the liner contracted, and to determine whether the bubbles have any effect on the inside surface. The thin Au layer on the inside surface allows us to characterize the z-dependent position of the inside surface of the liner, as described below.

The most rapid change in the film density with radial distance occurs very close to the radial location of the gold. This is because gold is a dense, high-Z material, compared with aluminum. This point of rapid change therefore corresponds to the radial position of the inside surface of the liner[5]. We have differentiated the data, determined the inflection point, and plotted this inflection point versus the z-coordinate in Fig. 6. The maximum z-dependent variations of the inside surface of the right edge of the liner are approximately 500 μm. Each bulge in the inflection point on the right edge of the liner corresponds with a low density bubble that is characteristic of the z-dependent instabilities, indicating that the bubble instabilities cause inward bulges on the inside surface of the liner. Only the larger bubbles affect the inside surface of the liner, smaller bubbles have little or no effect.

Conclusion

Flash radiography provides a wealth of information for dynamic experimentation generally, and for liner stability experiments specifically. In these liner stability experiments, the smoothness of the liner was a key issue. Flash x-ray radiography allowed us to quantitatively assess the smoothness of the liner as it imploded. The z-dependent bubble instabilities were observed to cause inward bulges on the inside surface of the liner. We have measured the wavelengths of the θ-dependent crenelation instability that grows on the inside surface of the liner, and have found the spectrum to contain a broad band of wavelengths.

In this paper, we have demonstrated x-ray system resolutions of up to four line pairs per mm. Improved resolution is always desirable. For these liner stability experiments, motion blur did not contribute significantly to the overall system resolution, because peak velocities were below 5 mm/μs. At higher velocities, it will become necessary to obtain x-ray pulse widths less than 10 ns, just to maintain the present system resolution. In our current configuration, both the penumbral blur and the x-ray-to-light converter systems conspire to limit our resolution. Efforts are currently being made to design and build sources with smaller spot sizes and shorter flash times with no appreciable loss of flux.

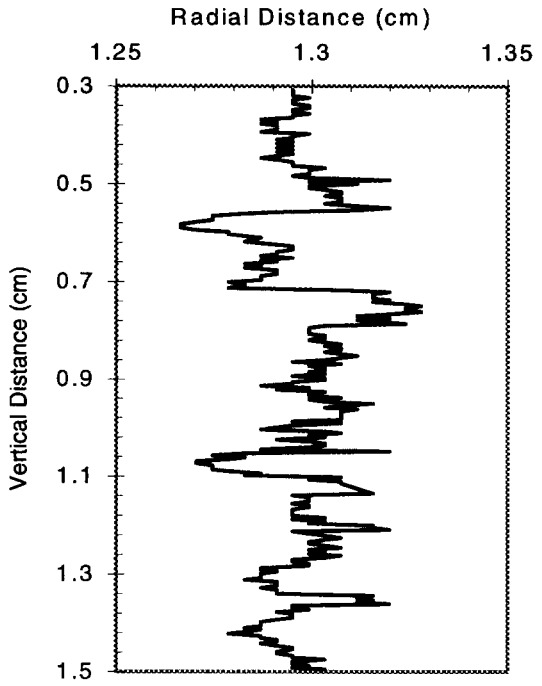

Fig. 6a. *The inflection point, which represents the inside surface of the liner, as a function of z.*

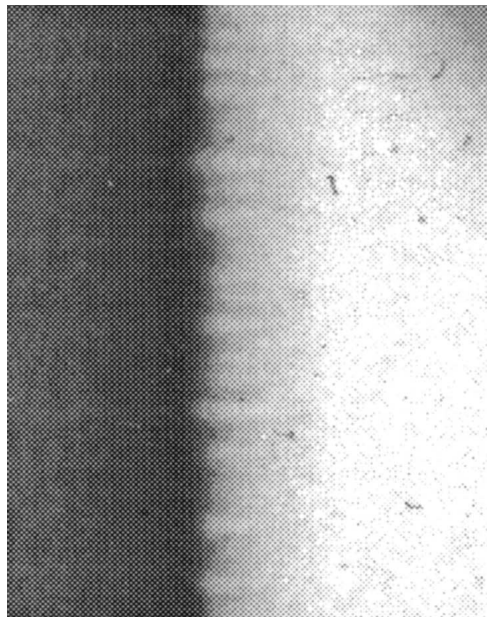

Fig. 6b. *LS-3 radiograph observed 8.5 μs after current start, with a peak current of 6.4 MA. The liner is at 58% of its initial radius. Note that the low density bubbles correspond with the inward bulges in Fig. 6a.*

REFERENCES

[1] W. J. Veigele in Handbook of Spectroscopy v. I, edited by J. W. Robinson (CRC Press, Cleveland, OH 1974), p. 28.

[2] D. Platts, M. P. Hockaday, D. Beck, W. Coulter, R. C. Smith, Proceedings of the 10th International Pulsed Power Conference, Albuquerque, NM, 1995, p. 892.

[3] Health Sciences Division, Eastman Kodak Company, Rochester, NY 14650.

[4] S. Watson, T. Kauppila, B. Haight, K Mueller, "Multiframe, High-Energy, Radiographic Cameras for Submicrosecond Imaging", LAUR-95-3570, 1995.

[5] B. Jahne, Digital Image Processing Concepts, Algorithms, and Scientific Applications, (Springer Verlag, Berlin, 1995), p. 134.